ELSEVIER

Journal of Nuclear Materials 266–269 (1999) 812–818

journal of nuclear materials

3D fluid modelling of the edge plasma by means of a Monte Carlo technique

Y. Feng *, F. Sardei, J. Kisslinger

Max-Planck-Institut für Plasmaphysik, EURATOM Association, D-85748 Garching, Germany

Abstract

An extended version of the 3D Monte Carlo edge plasma transport code EMC3 including more complex physics is presented. The balance equations for mass, momentum and energies are formulated in a general conservation form suited for direct application of the Monte Carlo solving algorithm. The new extended version is applied to the planned W7-AS island divertor. First results of the investigations, which are focused on neutral pump-out efficiency, power load distribution on the plates and high recycling performance, are presented. © 1999 Elsevier Science B.V. All rights reserved.

Keywords: Edge plasma; Simulation; Monte Carlo simulation; W7-AS

1. Introduction

In the last years, the urgent need of 3D transport models for understanding the divertor physics in a helical device such as W7-AS has become evident. A 3D Monte Carlo code (EMC3) [1], based on a simplified version of Braginskii's fluid equations [2], was developed in the last years and used successfully to interpret high recycling experiments in W7-AS island configurations [1,3,4]. However, the simplifications of the physical model (single fluid plasma ($T_e = T_i$), neglect of heat convection and parametric treatment of parallel momentum losses by using experimental data) restricted the code applicability so far. Recently, the EMC3 code has been extended substantially. The ion parallel momentum equation has been completed by including the cross-B viscous and convective transport of parallel momentum as well as the friction with neutrals provided by the neutral code EIRENE [5], which was coupled self-consistently to EMC3. In addition, the convective energy fluxes have been introduced into the heat balance equations and the electron and the ion energy transports were treated separately, which allows application of the code to low density plasmas, for which the electron temperature may largely differ from the ion temperature. The balance equations for mass, momentum and energies, which can be written into a general form, are treated with the same Monte Carlo algorithm, which solves both the diffusive and convective terms. The Monte Carlo procedure allows high flexibility in the 3D grid construction for both the plasma and plasma-facing components. An extension of the EMC3/EIRENE code to include impurity transport is under way.

Additionally, the code has been parallelized on the massive parallel computing system Cray-T3E (784 application processing elements at present), leading to a roughly linear, drastic speed-up of the computations.

2. The EMC3 code

The EMC3 code solves a set of Braginskii's fluid equations in a 3D space with a Monte Carlo technique. One of the main reasons for applying a Monte Carlo method is its high flexibility in the construction of the computational mesh. The magnetic islands and the discontinuous divertor plates in W7-AS and W7-X introduce a complex 3D edge structure. Owing to the shear of the diverted magnetic structures, the helical variation of the island shape and the strong anisotropy of the

* Corresponding author. E-mail: feng@ipp.mpg.de

PII: S0022-3115(98)00844-7

transports, the feasibility of a computational mesh acceptable for standard finite-difference methods is still an open question. The Monte Carlo method, on the other hand, allows high flexibility in construction and distribution of the computational mesh. Instead of solving a linear matrix for the unknown quantities at the grid points, the EMC3 code follows Monte Carlo particles, which undergo convective and diffusive processes in parallel and cross-field directions. If the magnetic field line vectors are defined everywhere, particles can be traced along and across the B-field lines through the edge plasma, independent on the mesh and coordinates selected. The computational cells are required just for scoring the Monte Carlo particles representing physical quantities such as mass, momentum and energy. Therefore, the grid can be locally adjusted according to the physical resolution.

2.1. Fluid model

We assume a simple neutral plasma consisting of electrons and a single ion species, i.e. $n = n_e = n_i$. The plasma transports are described by a simplifed time-independent version of Braginskii's fluid equations for particle, momentum and heat balance. In the absence of the electric field and plasma current, the equations for mass, momentum and energy read

$$\nabla_{||} \cdot nV_{||} + \nabla_{\perp} \cdot (-D\nabla_{\perp} n) = S_p, \tag{2.1}$$

$$\nabla_{||} \cdot \left(mnV_{||}V_{||} - \eta_{||}\nabla_{||}V_{||}\right) + \nabla_{\perp} \cdot \left(-m_i V_{||} D\nabla_{\perp} n - \eta_{\perp}\nabla_{\perp} V_{||}\right) = -\nabla_{||} P + S_m, \tag{2.2}$$

$$\nabla_{||} \cdot \left(-\kappa_i \nabla_{||} T_i + \frac{5}{2} n T_i V_{||}\right) + \nabla_{\perp} \cdot \left(-\chi_i n \nabla_{\perp} T_i - \frac{5}{2} T_i D \nabla_{\perp} n\right) = k(T_e - T_i) + S_{ei}, \tag{2.3}$$

$$\nabla_{||} \cdot \left(-\kappa_e \nabla_{||} T_e + \frac{5}{2} n T_e V_{||}\right) + \nabla_{\perp} \cdot \left(-\chi_e n \nabla_{\perp} T_e - \frac{5}{2} T_e D \nabla_{\perp} n\right) = -k(T_e - T_i) + S_{ee}, \tag{2.4}$$

where $p = n(T_i + T_e)$ and $\eta_{\perp} = m_i n D$. The signs $||$ and $\perp$ denote the components parallel and perpendicular to the magnetic field. The parallel transport coefficients $\eta_{||}$, κ_i and κ_e are considered to be classical, while the cross-B transports are usually assumed to be anomalous with D, χ_i and χ_e being determined from experiments. S_p and S_m are the ionization source and momentum loss via charge exchange with neutrals. In the present version, S_{ee} and S_{ei} represent the energy loss or gain of electrons and ions due only to the hydrogen neutrals. All the volume sources due to neutrals are provided by the EIRENE code.

The transport Eqs. (2.1)–(2.4) obey a generalized conservation principle. Introducing the dependent variable f standing for density, parallel velocity and ion or electron temperature, we can rewrite Eqs. (2.1)–(2.4) into a common Fokker–Planck form [6]

$$\nabla_{||} \cdot \left[\alpha_{||} f - \nabla_{||}\left(\beta_{||} f\right)\right] + \nabla_{\perp} \cdot [\alpha_{\perp} f - \nabla_{\perp}(\beta_{\perp} f)] = S, \tag{2.5}$$

where $\alpha_{||}$, $\beta_{||}$, $\alpha_{\perp}$, $\beta_{\perp}$ and S represent transport coefficients and source terms which are specific to a particular meaning of f (see Table 1).

In spite of the different structure of the boundary conditions for the mass, momentum and energy equations, the concept of the generalization of the fluid equations enables us to formulate a general numerical method, which can be used for determining the whole set of plasma parameters n, $V_{||}$, T_i and T_e.

2.2. Monte Carlo method

Eq. (2.5) describes the conservation of a physical quantity such as mass, momentum and energy during the convective and diffusive processes which can be simulated by following Monte Carlo particles. Particles are randomly generated according to a given source distribution and then followed in small time steps Δt. The corresponding random walk step, Δr, is determined by

$$\Delta r = \sqrt{2\beta_{||}\Delta t}\,\xi_{||} + \alpha_{||}\Delta t + \sqrt{4\beta_{\perp}\Delta t}\,\xi_{\perp} + \alpha_{\perp}\Delta t, \tag{2.6}$$

where $\xi_{||}$ and $\xi_{\perp}$ are the 1D and 2D random unit vectors parallel and perpendicular to B, respectively. The first and the third terms on the right hand side of Eq. (2.6) represent diffusion, the others convection of Monte Carlo particles in the two specific directions. Particles are traced and scored in a given mesh. If a particle is lost to target plates or to other sinks, a new particle is started and the computation continues until the desired statistical accuracy is achieved. Finally, the distribution function f is given by

Table 1
Meaning of the symbolic transport coefficients and sources associated with f

f:	mass n	momentum $V_{||}$	heat $T_{e,i}$
$\alpha_{||}$:	$V_{||}$	$m_i n V_{||} + \nabla_{||}\eta_{||}$	$\frac{5}{2} n V_{||} + \nabla_{||}\kappa_{e,i}$
$\beta_{||}$:	0	$\eta_{||}$	$\kappa_{e,i}$
$\alpha_{\perp}$:	0	0	$(\chi_{e,i} - \frac{5}{2} D)\nabla_{\perp} n$
$\beta_{\perp}$:	D	$m_i n D$	$n\chi_{e,i}$
S:	S_p	$-\nabla_{||} p + S_m$	$\pm k(T_e - T_i) + S_{ee,i}$

$$f = \frac{Q_s}{Q_v}\left(\frac{\Delta N_p}{N_p}\Delta t\right), \tag{2.7}$$

where N_p is the total number of the particles followed and ΔN_p is the number of particles scored in the volume element Δv. Q_s is the total source strength including the contributions of volume sources and surface sources specified on the boundary.

The time step Δt appearing in Eqs. (2.6) and (2.7) does not, of course, mean that the solution of the problem depends on the time step chosen in the computation. In fact, the quantity $(\Delta t \Delta N_p)/N_p$ is just the average time interval spent by the particles to travel through the volume element Δv. This quantity is completely determined by the transport coefficients, source distributions and boundary conditions. As long as the time step is kept sufficiently small, it has no effect on the final solution.

2.3. Computational mesh

An optimal choice of the computational mesh is essential to improve the computation performance. Two points have to be considered in the mesh construction. First, a mesh is needed to store the Monte Carlo particles representing physical quantities such as density, velocity and temperatures. The transport coefficients listed in Table 1 depend strongly on such quantities. Due to both the high non-linearity of the equations and the large difference between the parallel and perpendicular transports, a non-uniform cell distribution is necessary to meet the physical requirements. Secondly, for tracing Monte Carlo particles the magnetic field lines need to be specified. The mesh should be able to accurately define them, in order to avoid a time-consuming integration procedure for the field lines of the individual particles. According to these considerations, we choose magnetic coordinates for particle tracing as they allow a simple representation of the B-field lines. However, due to the large number of the grid points needed to describe the complex magnetic surface geometry, storage problem will emerge if the plasma parameters are based on the same mesh. Therefore, in order to reduce the memory and to speed up the computations, two different meshes are defined, the basic geometric mesh for tracing particles and a coarser physical mesh for representing plasma parameters, which can be locally adjusted according to the required resolution.

Fig. 1 illustrates the cell distributions of an $\iota = 5/9$ W7-AS configuration at a cross section of a lower divertor. The basic geometric mesh consists of about 200 000 grid points, covering a half period of the edge

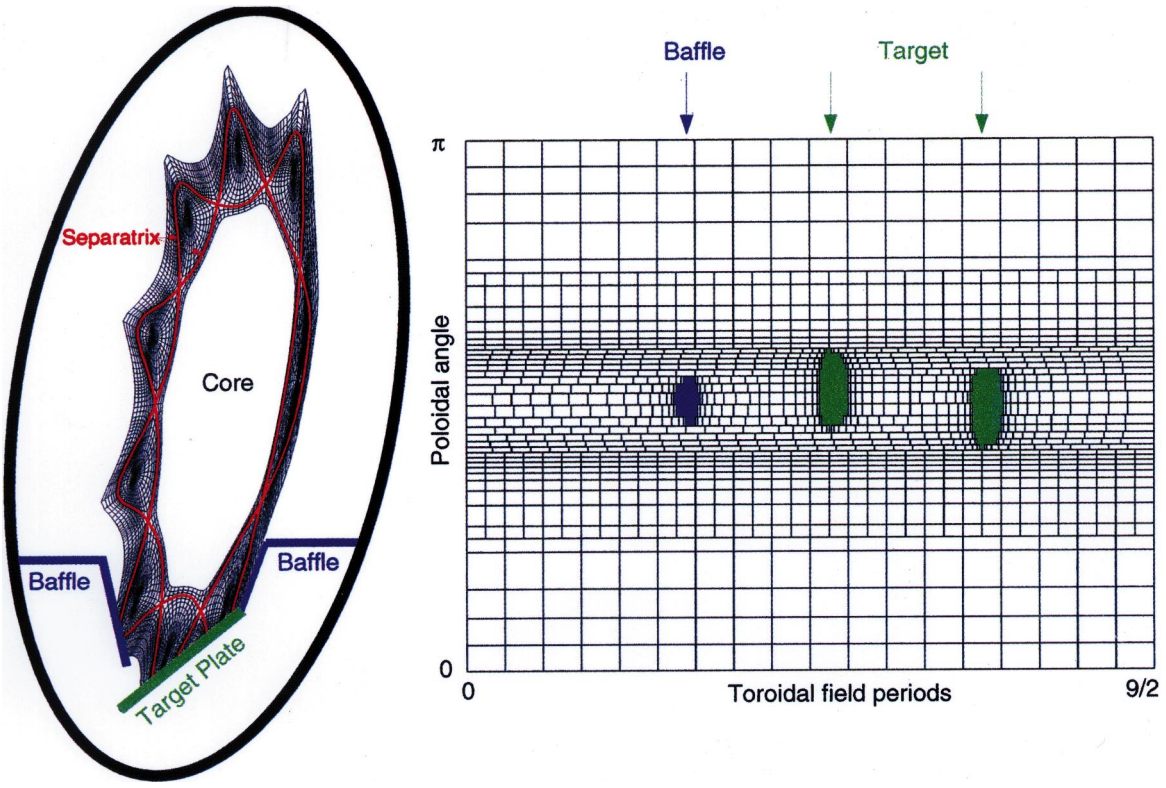

Fig. 1. 3D grid distributions for a 5/9 island divertor configuration.

configuration, according to the stellarator symmetry in W7-AS. The grids on each cross section are adjusted as to meet both the geometrical and physical requirements. The toroidal geometric grids, on the other hand, are constructed uniformly and then reduced to give a non-uniform subset which represents the physical mesh satisfying the required resolution, for example, finer cells at the plates (right figure).

In order to speed up the computation, it is necessary to represent the target plates in the magnetic coordinates as well.

3. Applications

Calculations are based on the divertor configuration given in the previous section. Pure hydrogen plasma is assumed with a total power outflow of 400 kW through the separatrix. This power is kept constant for all calculations. The edge plasma density is varied by increasing the total particle outflow to the targets. The diffusion coefficients are kept spatially constant, however scaled with the average edge density roughly as $1/\langle n\rangle_{\mathrm{sol}}$, with $\chi_e = \chi_i = 2D$. Radial decay lengths of 2 and 4 cm are set on the last radial surface for the density and temperatures. Momentum entering the plasma core is absorbed, which corresponds to a boundary condition of $V_{||} = 0$ at the innermost surface contacting the main plasma. Bohm's boundary conditions are assumed at the plates. All source terms due to neutrals are calculated by the EIRENE code.

3.1. Low and high recycling

Two density cases resulting from the given particle fluxes of 6.25×10^{21} s^{-1} and 2.5×10^{22} s^{-1} to the targets are compared in Fig. 2, which shows the temperature and density distributions on a cross section cutting the lower divertor plates. The diffusion coefficient D is taken to be 1 m^2/s for the lower density case and decreases to 0.25 m^2/s as the density increases. Despite the small pitch angle of the magnetic field lines inside the islands, the parallel heat conduction dominates the energy transport for electrons, which is indicated both by the energy flux diversion and the weak dependence of the electron upstream temperature on the density. The ion energy transport, on the other hand, is governed by the cross-B anomalous heat conduction due to the weak parallel conductivity, especially in the higher density case. The electron and ion downstream temperature, $T_{e,down}$ and $T_{i,down}$, decrease from 24 and 39 eV to 9 and 12 eV as the density increases, which are still high enough for ionization of neutrals. Thus, no significant momentum losses via charge exchange contribute to the momentum balance. A very important momentum loss mechanism instead is the cross-B momentum transport resulting from the enhanced anomalous cross-B diffusion of the ions. Because of the large ratio of the connection length to the island size, perpendicular particle diffusion dominates over parallel convection in a large island region away from the targets. Momentum loss occurs if the ions exchange their momentum through diffusion inside the islands. For the lower recycling case, neutrals penetrate deeply into the islands, causing a monotonous radial drop of the density profile. Density increases with increasing recycling flux, especially at the downstream position close to the targets. The increasing density shifts the ionization zone outwards and decreases the down-stream temperatures, leading to a density rise in front of the targets. Toroidally away from the targets, the density peak is smoothed by diffusion, resulting in a rather broad density profile in the island SOL between the targets.

3.2. Energy and particle exhaust

Control of the energy and particle exhaust is the basic task of the island divertor, where the energy flux density to the plates must be kept below a technical limit. For the planned W7-AS divertor, ten discontinuous divertor plates are installed up-down symmetrically on the elliptical cross sections with a toroidal extension of 18 degrees each. Each divertor plate cuts poloidally two islands so that the ten plates cover a total toroidal length comparable to the single null divertor in a tokamak of the same size. However, unlike in tokamaks, the complex magnetic island structure introduces a 2D distribution of the power load on each target, which can only be studied by a 3D model, for example the EMC3 code.

Fig. 3 shows the power load distribution on a target for the high density case, which does not differ significantly from the low density case because of the inverse dependence of the cross-B transport coefficients on the density. A large portion (84%) of the heating power is convected to the plates while the rest is radiated by neutrals. Energy flows along island fans to the targets, resulting in poloidally peaked profiles of the power load with a maximum of 1.7 MW/m^2 at the position of the largest connection length. Toroidally at the plate centre two tiles are introduced for diagnostic purposes, which are retracted in order to avoid direct exposure to the plasma. This explains why the power load distribution in ϕ direction is strongly inhomogeneous. The plates are optimized to allow operations of W7-AS with different magnetic configurations covering a wide ι range. In practice, for a given configuration, the power load distribution can be smoothed by twisting the plates poloidally. This, however, would restrict the operating configuration range.

In order to reach a steady-state operation at the presence of NBI heating the injected particles must be pumped out in the divertor. Neutrals are compressed in

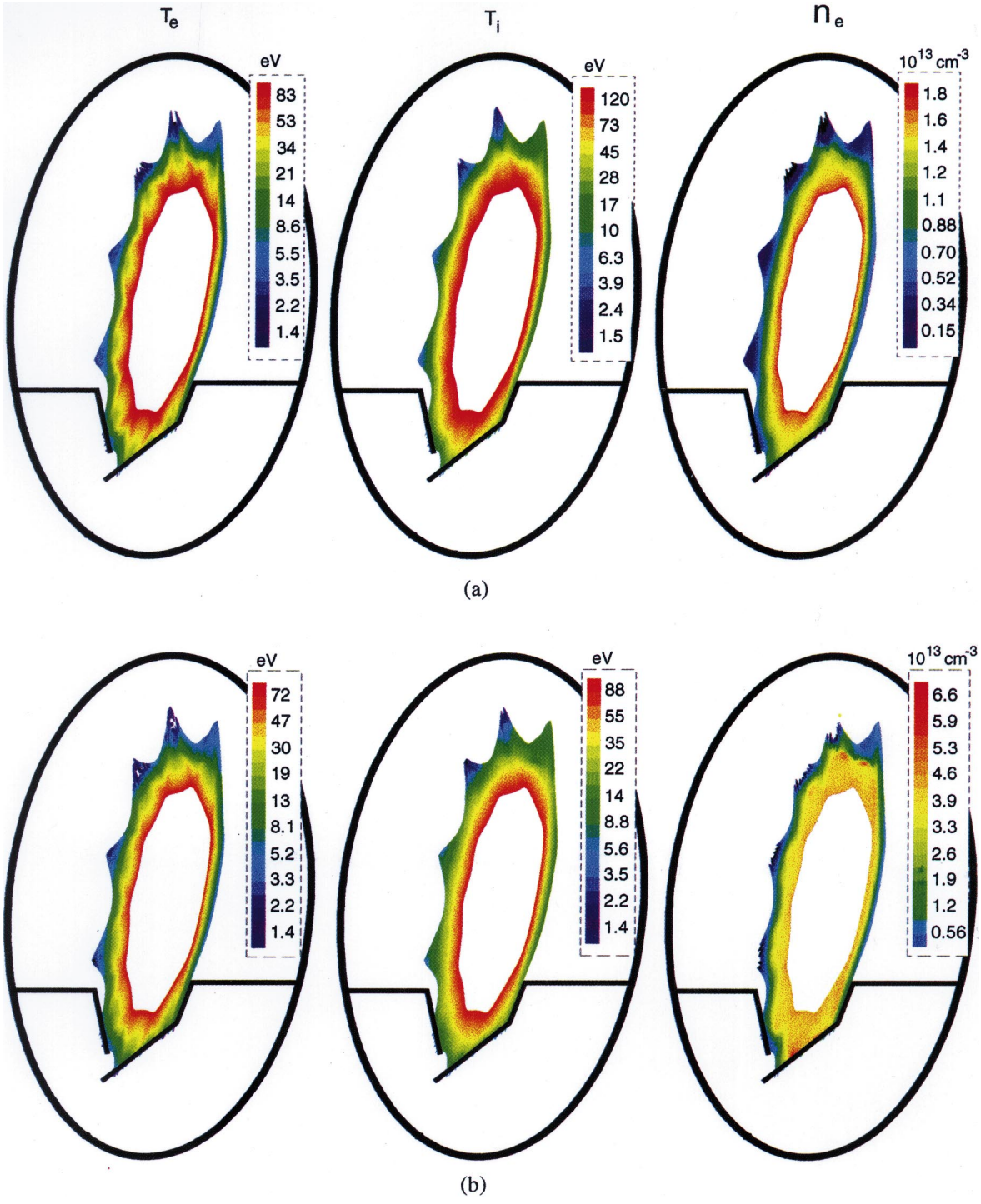

Fig. 2. 2D distributions of the electron and ion temperatures and the density at the cross section of a lower divertor target for the particles fluxes of (a) 6.25×10^{21} and (b) 2.5×10^{22} s^{-1}.

divertor chambers in which titanium gettered plates are mounted for absorbing the incoming neutrals. Fig. 4 shows the distributions of the ionization rate, atom and molecule densities for the high recycling case. Ions flowing onto the targets are partly reflected as atoms and the rest is absorbed and emitted as cold molecules. The

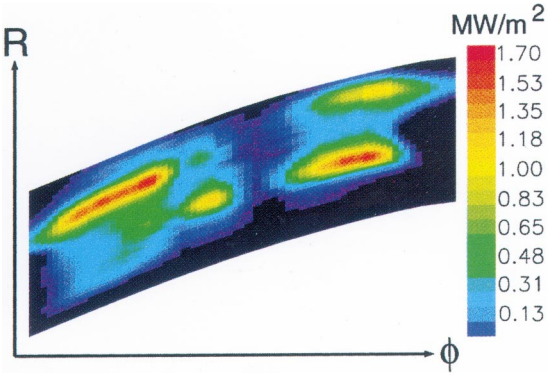

Fig. 3. Power load distribution on a target for the high density case where R and ϕ indicate the radial and toroidal directions.

neutrals can directly enter the divertor chamber or indirectly through charge exchange with ions inside the islands. Reflection between the walls in the divertor chamber leads to reduction of the atom fluxes in favor of cold molecules, resulting in much higher densities for molecules than for atoms.

For a given absorbing area of the titanium plates (about 1.8 m^2 in total), the pumping speed is determined by the sticking probability and the influx of the neutrals into the divertor chamber. The dependence of the pumping speed on the divertor gap is shown in Fig. 5(a), in which the sticking probability for hydrogen atoms, due to lack of a reliable knowledge, is varied from 2% to 10% while for molecules it is fixed to be 2%. For a very narrow divertor gap (<2 cm), all the neutrals coming into the chamber are absorbed by the titanium plates, showing a roughly linear dependence of the influx on the width of the divertor gap. With increasing gap width, more and more neutrals will escape from the chamber without being absorbed, which moderates the increase of the pumping speed and may even lead to decrease in pumping speed if the gap becomes too wide. The optimal width is about 5 cm, slightly depending on the sticking probability. In this case, the pumping speed reaches a value of 4×10^{20} s^{-1} if the same sticking probability of 2% is assumed for both atoms and molecules. This allows a NBI heating power of 2 MW for the neutral particle injectors on W7-AS. Higher heating power (3.5 MW available) will increase the plasma edge density.

If the sticking probabilities for atoms and molecules are comparably small, more molecules are pumped out than atoms, as shown in Fig. 5(b). The pumping speed for atoms will exceed that for molecules if the atoms have a sticking probability higher than 7%.

4. Conclusions

The physical model in the EMC3 code has been greatly improved. The anomalous cross-B momentum transport terms are introduced which are found to give dominant contributions to the momentum balance due

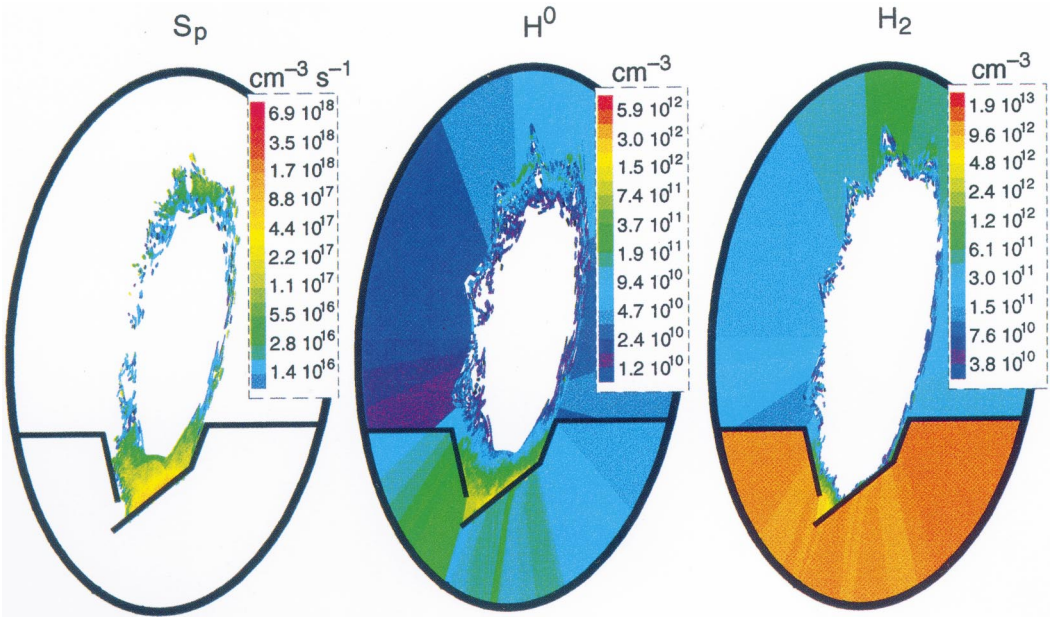

Fig. 4. 2D distributions of the ionization rate and atom and molecule density at the cross section of a lower divertor chamber for the high density case.

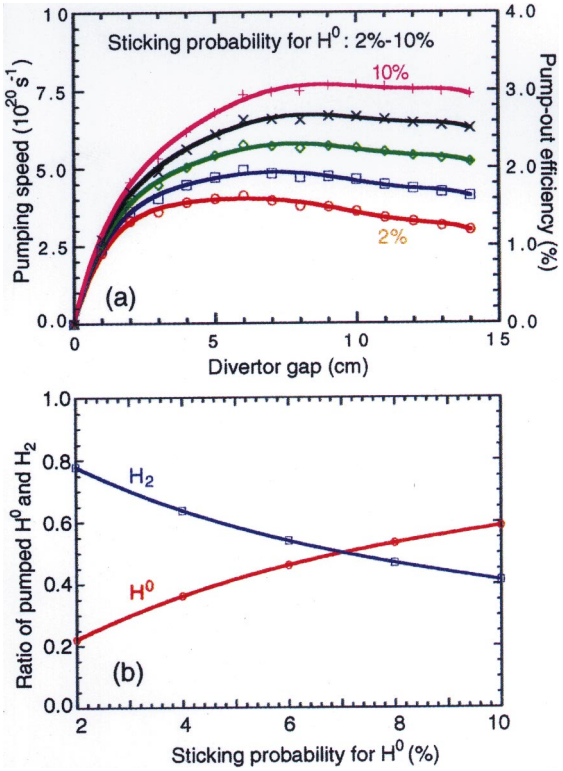

Fig. 5. Dependence of the pumping speed on the divertor gap width (a) and the ratio of the pumped atoms and molecules as a function of the atom sticking probability (b).

to the small pitch angles of the magnetic field lines in the islands. Separation of the electron and ion energy transports and introduction of the corresponding convective energy fluxes considerably extend the application range. All the fluid equations obey a same conservation principle, and are therefore treated with the same Monte Carlo algorithm. Parallelization of the EMC3 code leads to a roughly linear speed-up of the computations.

Simulations show that the anomalous cross-B transports play an important role in the mass, momentum and ion energy balance. Increasing the plasma edge density shifts the ionization zone outwards, leading to a density rise in front of the targets. Toroidally away from the recycling zones, the anomalous diffusion smooths the density distribution, resulting in a rather broad density profile in the edge. Calculations show inhomogeneous distributions of the power load on the targets. In the absence of impurities, 84% of the 0.4 MW heating power entering the island SOL is convected to the divertor plates, with a maximal energy flux of 1.7 MW/m^2 localized at the position of the largest connection length. Neutrals are well confined in the divertor chamber with a 5 cm divertor gap being the optimal choice for pumping out the neutrals. For an average edge density of 4×10^{19} m^{-3}, a pumping speed of 4×10^{20} s^{-1} is achieved, which allows a steady-state operation with NBI heating up to 2 MW. Higher heating power will increase the plasma edge density.

References

[1] Y. Feng et al., J. Nucl. Mater. 241–243 (1997) 930.
[2] S.I. Braginskii, M.A. Leontovich (Ed.), Reviews of Plasma Physics, vol.1, Consultants Bureau, New York (1965) 205.
[3] F. Sardei et al., J. Nucl. Mater. 241–243 (1997) 135.
[4] P. Grigull et al., J. Nucl. Mater. 241–243 (1997) 935.
[5] D. Reiter, Jülich Report 1947, Jülich (1984).
[6] N.G. Van Kampen, Stochastic Processes in Physics and Chemistry, North-Holland, Amsterdam, 1981.